Brodogradnja Volume 76 Number 4 (2025) 76406

journal homepage: www.brodogradnja.fsb.hr

Brodogradnja

An International Journal of Naval Architecture and Ocean Engineering for Research and Development

Numerical study of scale effects of viscous roll damping for a container ship

Nguyen Thi Ha Phuong[1,2*], *Tomoki Taniguchi*[1], *Toru Katayama*[1]

[1] *Department of Marine System Engineering, Graduate School of Engineering, Osaka Metropolitan University, 599-8531 Osaka, Japan*
[2] *Faculty of Shipbuilding, Vietnam Maritime University, 18000 Hai Phong, Vietnam*

ARTICLE INFO

Keywords:
Scale effects
Full-scale roll motion
Roll decay
Forced roll
Roll damping coefficient
Bilge-keel component

ABSTRACT

In this paper, the scale effects on a container ship's roll motion are investigated by numerical approach. The accuracy of the numerical method is verified by comparing numerical results with experimental data through a grid sensitivity study. The roll decay tests of the vessel at full-scale and model-scale at various forward speeds are simulated, and it is noticed that scale effects on roll motion occur when forward speed is nil or low. To further understand the impacts of scale on damping components, forced roll tests with different forward speeds are simulated, roll damping coefficients are determined, the flow field created by roll motion and forward speed near bilge keels is observed. It is found that the scale effects affect both the frictional and bilge keel damping components. At low Froude number, the difference of the relative velocity distributions for the height (or breadth) of bilge keels between model (model-scale) and ship (full-scale) is proved as the cause of the scale effects on the bilge keel component.

1. Introduction

Normally, ship roll motion is obtained as model scale data by towing tank test or numerical simulation. However, scale effects exist due to the discrepancy in the Reynolds number of the vessel at different scales. While collecting sea trial data is difficult, computer technologies like Computational Fluid Dynamics (CFD) currently becomes a useful solution to simulate full-scale roll motion. As a result, precisely predicting roll motion using numerical methods is critical for investigating the scale effects on roll motion.

For many years, many attempts have been made to solve the problems related to scale effects. Zhang et al. [1] predicted the resistance and motions for the ship DTMB 5415 at model and full scales by numerical simulation. With the same ship, Song et al. [2] investigated the scale effects on its hydrodynamic performance in the case of using a stern flap. Using CFD, the scale effects on each component of resistance of two vessels (KVLCC2 and KCS) were examined by Dogrul et al. [3]. In another paper by Dogrul [4], scale effects were analysed for a submarine but focused on propulsion tests. Ma et al. [5] studied the impact

* Corresponding author.

E-mail address: phuongnth.dt@vimaru.edu.vn

http://dx.doi.org/10.21278/brod76406

Received 29 January 2025; Received in revised form 3 June 2025; Accepted 8 July 2025

Available online 2 August 2025
ISSN 0007-215X; eISSN 1845-5859

of scale on the flow field for a container vessel in shallow water. In these studies, not only were the scale effects revealed, but also the in-house CFD has proven its reliability in predicting full-scale simulation. However, these works mostly focus on the scale effects in the aspect of ship resistance and propulsion, while in respect of rolling motion, they are rare. Grant [6] conducted the sea trial roll decay tests for a combatant vessel in calm water to collect full-scale results of bilge keel force and measure the flow fields at various speeds. For further development, Broglia et al. [7] analysed roll decay motion of this vessel by means of sea trials, model scale experiments and numerical simulations at various speeds and scales. Despite a larger difference between full-size and model-size roll amplitude being observed at low Froude number, the scale effects were unclear, as well as computer simulations underpredicting the roll decay motion for low speed because of the lack of mesh resolution. It was shown in a paper by Söder et al. [8] that the full-scale roll amplitude was marginally larger than the model-scale one, which required more study. Kianejad et al. [9] used the harmonic exciting roll motion (HERM) technique to analyse the scale effects on roll motion for a container ship. Despite the discrepancies in rolling motion at different Reynolds numbers shown in these studies using diverse approaches, there are still many problems pertaining to scale effects that need to be investigated. These studies only focused on roll decay motion to investigate the scale effects, whereas their influence on different components related to roll damping is still questionable. Ikeda et al. [10] proposed a semi-empirical method to estimate five roll damping components based on some theoretical considerations and the experimental results. During the process of improving Ikeda's method, Katayama et al. [11] found that the scale effects occurred on the bilge keel component related to the bilge keel breadth. However, this finding was based on investigating the model test data at different Reynolds numbers, no comparison between model-scale and full-scale and the reason for that phenomenon have not been given. In a previous study by the authors [12] on a light combatant vessel (Bettica ship) with a slender-shape hull and sufficiently long bilge keel breadth at model-scale and full-scale, the scale effects on roll motion were detected. Especially, the bilge keel damping component was found to be different between model-scale and full-scale when the bilge keel breadth was reduced to a half. Although scale effects on roll damping components were discovered more obviously, the explanation of the underlying causes remained incomplete.

Therefore, using a numerical approach, this study aims to more deeper analyse the scale effects on roll motion using a container ship with a round-shape hull and short bilge keel breadth named Duisburg Test Case (DTC). The reasons for the scale effects on roll damping components are explained through observed the flow fields. The article is organized as follows: firstly, the roll decay tests of the DTC ship equipped with bilge keels and a rudder at different scales are numerically simulated. Then, a mesh sensitivity study is presented, and the reliability of the numerical results is confirmed through comparing them to the experimental data. After that, the scale effects are detected by comparing the roll decay amplitudes of full-scale with model-scale at different forward speeds. To clarify the impacts of scale on damping components, forced roll tests with different forward speeds are simulated, then roll damping coefficients are determined. Finally, the velocity fields and velocity vectors near the bilge keel area as well as the relative velocity distributions are analysed, and the cause of the scale effects is explained in detail.

2. Simulation

2.1 Hull geometry and data

A post-panamax container vessel with the name as DTC is chosen as the research object in this paper. Belonging to the Institute of Ship Technology, Ocean Engineering and Transport Systems (ISMT), this vessel's experimental data was used to benchmark and validate the numerical computations. The vessel has a rudder and five bilge keels on each side. Each bilge keel segment measures 14.85 meters in length, 0.4 meters in height (or breadth) and the thickness of its tip is 0.02 meters. Figure 1 illustrates the hull geometry of DTC vessel and Table 1 provides its main characteristics at full-scale and model-scale. More details about the hull design and model test data for roll decay motion, propulsion, and resistance can be found in [13].

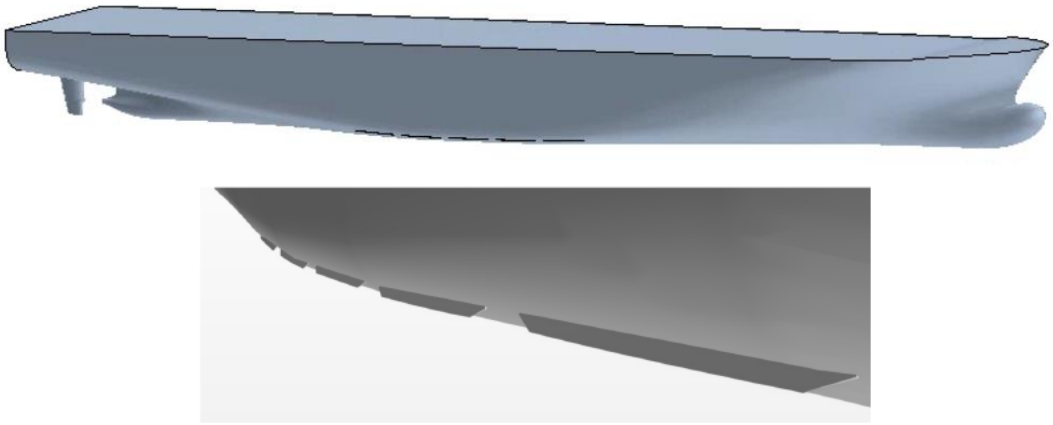

Fig. 1 Hull geometry of DTC vessel

Table 1 Main particulars of DTC vessel

Parameters	Symbol	Ship	Model
Scale ratio	-	1	1/59.407
Water line length (m)	L_{WL}	360.9	6.069
Length between perpendiculars (m)	L_{pp}	355.0	5.976
Breadth (m)	B	51.0	0.858
Draft (m)	d	12.0	0.202
Block coefficient	CB	0.628	0.628
Mass (t)	M	140,033.0	0.650
Metacentric height (m)	GM	4.57	0.077
Roll radius of gyration in X direction (m)	k_{xx}	19.39	0.326
Pitch and yaw radius of gyration in Y, Z direction (m)	k_{yy}, k_{zz}	95.86	1.614
Natural roll period (s)	T_r	20.36	2.6

2.2 Computational setting

The numerical approach mentioned in this paper is applying a CFD tool called Star-CCM+, which bases itself on solving the equations of fluid motion in simulating and predicting the rolling motion. In this paper, the finite volume approach is used to discretize the transport equation in order to solve unsteady Reynolds-Averaged Navier-Stokes equations. Using the Volume of Fluid (VOF) method, the free-surface interface between air and water is simulated using a two-phase interface capturing technique. The Shear Stress Transport (SST) k-ω model is chosen for all cases due to its accuracy in respect of flow physics and numerical stability as shown in previous studies [14, 15] and especially in the roll motion simulation [16-18]. The SST k-ω model effectively captures near-wall behavior in turbulent flows, including at full-scale (where the flow is fully turbulent), using a blending function to switch between the k-ω and k-ε models. It activates the k-ω formulation near the wall, where it excels at accurately predicting turbulence, and switches to a k-ε formulation in the free stream, where it is more robust. This hybrid approach provides accurate predictions of turbulent kinetic energy and dissipation rate. The SST k-ω model's ability to effectively handle the transition between the k-ω and k-ε formulations allows it to accurately predict the

turbulent kinetic energy and dissipation rate throughout the entire flow field, including the near-wall region [19, 20].

As the overset mesh method has more advantages than other meshing approaches, which was proved in a paper by Irkal et al. [21], it is used in this work to predict roll motions at different Reynolds numbers. The computational domain comprises background and overset regions, in which the overset region rotates around the ship's longitudinal axis to imitate the rolling behavior. The overset region is coupled with the background region through an overset interface using layered hole-cutting approach. Linear interpolation scheme is used to transfer data between meshes, in which donor cell values are interpolated to provide data for acceptor cells. The overset cell status of the background mesh is described in Figure 2. The background (the tank) is a rectangular prism whose dimensions are sufficiently large for preventing the reflection of waves. The dimensions of overset and background regions are chosen based on reference to the computational domain size in previous studies on roll motion simulation [22, 23]. The dimensions of calculation regions and the physical conditions applied to boundaries are given in Figure 3.

For both computational regions, the hexahedral mesh is generated using different meshing models: trimmer mesh, surface remesher, and prism layers. Meshes are refined in necessary areas (near the hull, bow, stern, rudder and bilge keels) using separate refinement blocks aimed at capturing more flow details and simulating the roll decay motion more exactly (see Figure 4). As the SST k-ω turbulence model is used, the wall y+ of model-scale should be within 2.5 following the guidance of ITTC [24]. On the other hand, wall y+ of full-scale should be within 200 as suggested in many studies [25-29]. An example of wall y+ contours for medium mesh of different cases is shown in Figure 5.

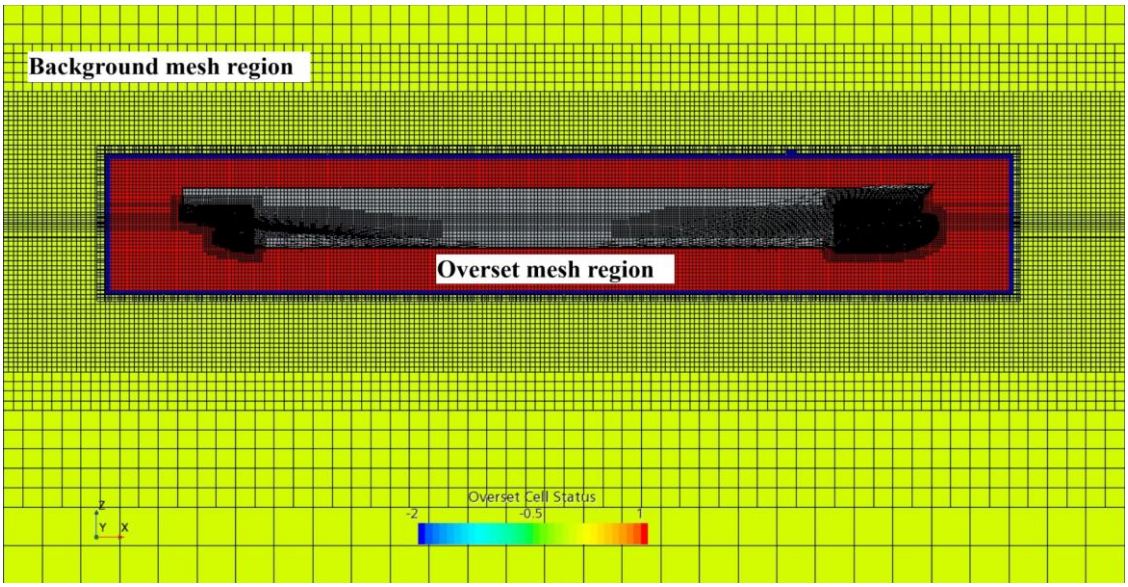

Fig. 2 Overset cell status of background mesh (yellow: active cells; dark blue: donor cells; red: inactive cells)

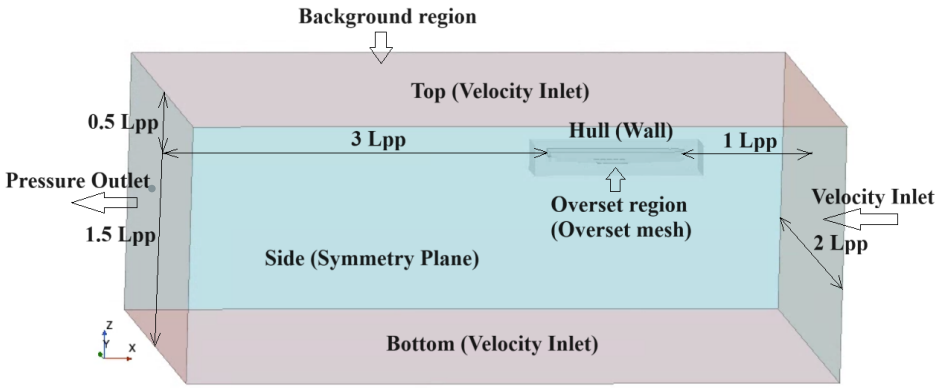

Fig. 3 Domain dimensions and boundary conditions

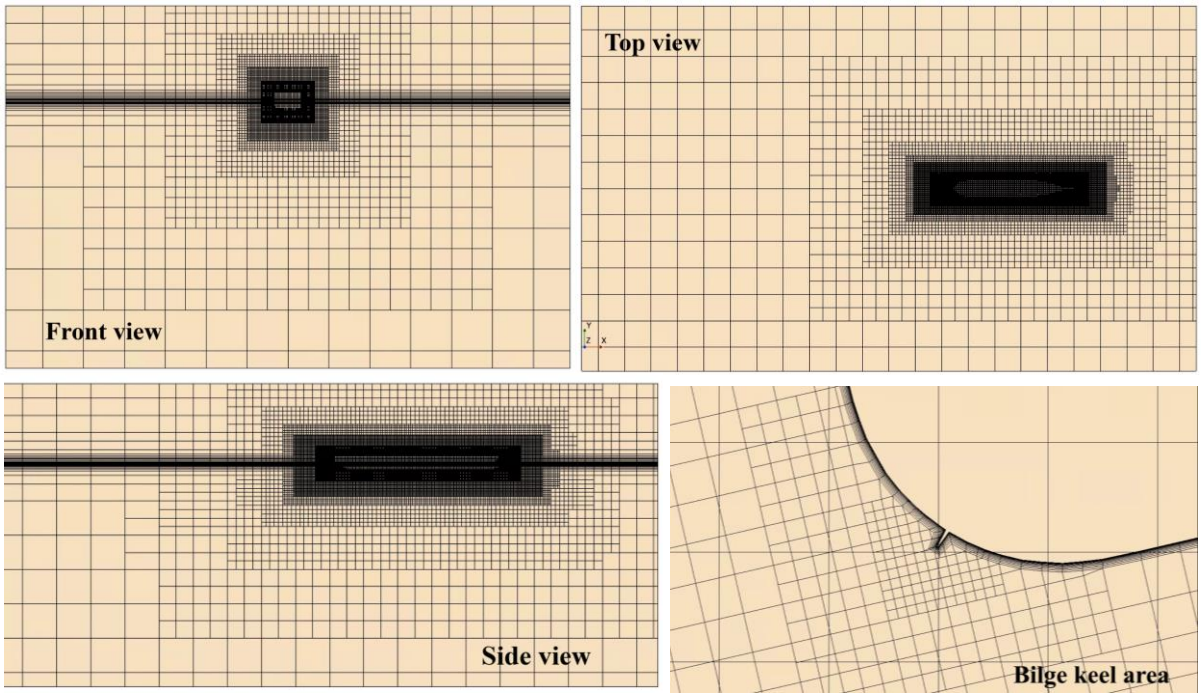

Fig. 4 Mesh refined in different locations of DTC ship

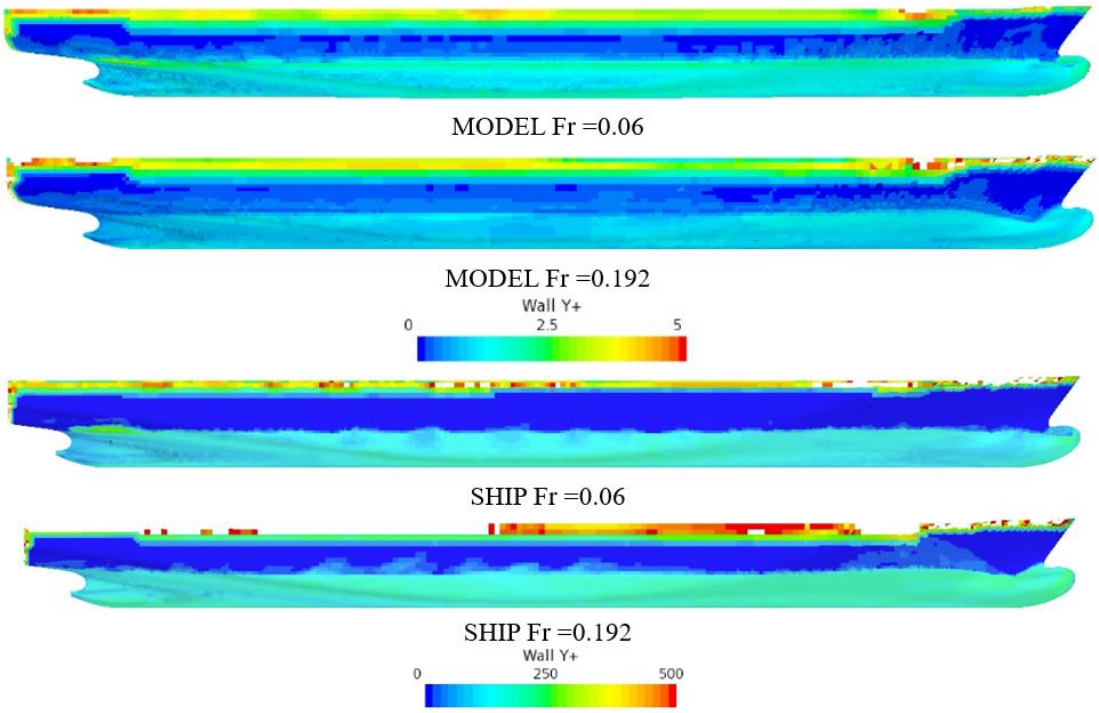

Fig. 5 Wall *y*+ contours for the medium mesh

Following the recommendation of ITTC [24], "for periodic phenomena (e.g., roll decay, vortex shedding, incoming waves, etc.) use at least 100 time steps per period". In the present study, a time step considering the Courant number, which is much smaller than the ITTC recommendation, is used to ensure the accuracy of numerical results. Hence, the time step should be chosen so that the Courant number on the ship surface is less than 1.0. By setting different time steps for the simulation and checking the Courant number on the ship hull surface after some runs, the suitable time step can be chosen. Therefore, the defined time steps for DTC ship are selected as 0.01 s (= T_r/250) and 0.07 s (= T_r/290) for the model-scale and full-scale simulations, respectively.

3. Verification and validation

3.1 Mesh convergence study

In CFD simulation, uncertainty analysis is necessary to verify the reliability of numerical results. Theoretically, the errors caused by input parameters are mostly errors in mesh size, time step and iteration number. In this study, the uncertainty calculated from the iteration number can be ignored as the simulation condition is in calm water. As suitable time step has already been determined as mentioned above, only mesh size is considered as a primary source of uncertainty.

The mesh convergence study is conducted using Grid Convergence Method (GCI), which was introduced by Roache [30], and detailed descriptions of the verification procedure can be seen in the guidelines document of ITTC [31]. Three mesh solutions are created, and the details of study cases for both model-scale and full-scale are given in Table 2. A refinement ratio of $r_i = \sqrt{2}$ is applied for both scales as "it provides fairly large parameter refinement ratio and at least enables prolongation of the coarse-parameter solution as an initial guess for the fine-parameter solution" [31]. This allows for a sufficient difference in grid density to effectively capture the discretization error while keeping the number of simulations manageable. Convergence ratio (R_i) is defined through the variation of numerical results for fine ($S_{i,1}$), medium ($S_{i,2}$), and coarse ($S_{i,3}$) solutions as follows:

$$R_i = \varepsilon_{i,21} / \varepsilon_{i,32} \tag{1}$$

$$\varepsilon_{i,21} = S_{i,2} - S_{i,1} \tag{2}$$

$$\varepsilon_{i,32} = S_{i,3} - S_{i,2} \tag{3}$$

Depending on the value of R_i, the following cases can occur: monotonic convergence ($0 < R_i < 1$), oscillatory convergence ($R_i < 0$; $|R_i| < 1$), monotonic divergence ($R_i > 1$) and oscillatory divergence ($R_i < 0$; $|R_i| > 1$). For monotonous convergence, the generalized Richardson extrapolation can be applied to calculate numerical uncertainty (see [30] for more details). The order of convergence rate (p_i), the normalized discretization error in the solution ($\delta^*_{RE\,i,1}$), the grid convergence index (GCI) and corrected uncertainty (U_{ic}) are defined as follows:

$$p_i = \frac{ln(\varepsilon_{i,32} - \varepsilon_{i,21})}{ln(r_i)} \tag{4}$$

$$\delta^*_{REi,1} = \frac{\varepsilon_{i,21}}{r_i^{p_i} - 1} \tag{5}$$

$$GCI^{21} = \frac{F_s \delta^a_{i,21}}{r_{i,21}^{p_i} - 1} = F_s \left| \delta^*_{REi,1} \right| \tag{6}$$

$$U_{ic21} = (F_s - 1) \left| \delta^*_{REi,1} \right| \tag{7}$$

where F_s represents the factor of safety.

For roll decay simulation, extinction coefficients are calculated based on the results of three mesh solutions to calculate the convergence ratio. This approach was used in a study by Yang Bo et al. [32] and has been confirmed to be reliable with the initial roll angle under 20 degrees. From the roll decay curve, the peak values of the roll amplitude ϕ_k, ϕ_{k+1} can be defined, and the extinction curve $\Delta\phi = f(\phi_m)$ could be estimated according to Equation (8):

$$\Delta\phi = \phi_k - \phi_{k+1}; \phi_m = (\phi_k + \phi_{k+1}) / 2 \tag{8}$$

For small initial roll angles, extinction coefficient ($2\mu_{\varphi\varphi}$) can be calculated by:

$$2\mu_{\phi\phi} = \frac{2}{\pi} \cdot \frac{\Delta\phi}{\phi_m} \tag{9}$$

The model-scale and full-scale results of the mesh convergence study are given in Table 3. Roll decay curves of different study cases are described in Figure 6 and Figure 7. The results show that monotonic convergence is obtained, and the uncertainty values are small. The calculated order of accuracy is reasonable. In addition, the grid convergence index $GCI^{21} < GCI^{32}$ means that the discretization error from the grid size is decreased, resulting in an independent solution. The roll amplitudes simulated by fine mesh and medium mesh are mostly the same, which means that the medium mesh is accurate enough.

Table 2 Mesh convergence study cases

Model-scale (Full appendages, F_r = 0, initial roll angle = 15.2°)			
Mesh type	Base size (m)	Grid cells (mil. cells)	Time step (s)
Coarse	0.2	1.7	0.01
Medium	0.16	2.7	0.01
Fine	0.12	5.2	0.01
Full-scale (Full appendages, F_r = 0, initial roll angle = 15.2°)			
Mesh type	Base size (m)	Grid cells (mil. cells)	Time step (s)
Coarse	9.6	2.2	0.07
Medium	7	4.8	0.07
Fine	5	11.5	0.07

Table 3 Results of mesh convergence study

Parameters	Model-scale	Full-scale
$S_{i,1}$	0.072	0.063
$S_{i,2}$	0.074	0.064
$S_{i,3}$	0.083	0.068
R_i	0.246	0.253
p_i	4.050	3.960
GCI^{21}	0.250	0.126
GCI^{32}	0.989	0.488
U_{ic21} (%)	1.252	0.628
U_{ic32} (%)	4.944	2.440

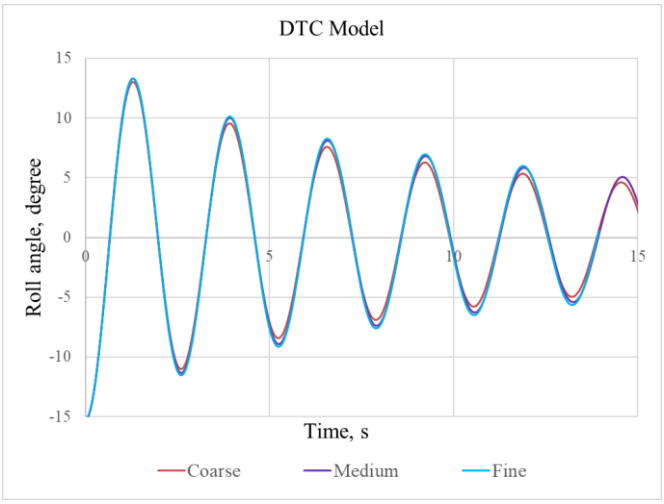

Fig. 6 Mesh convergence study at model-scale

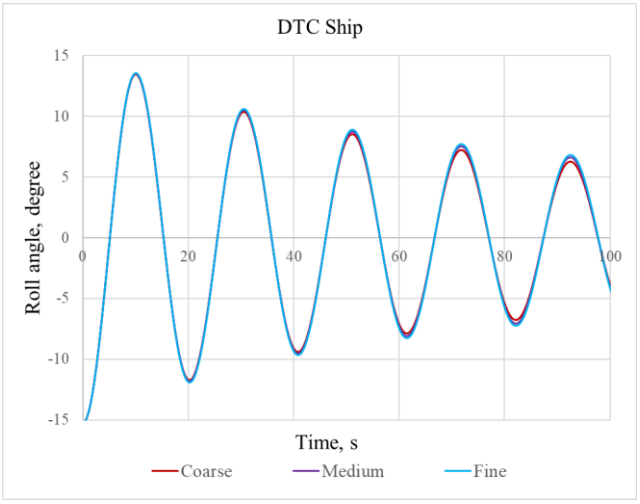

Fig. 7 Mesh convergence study at full-scale

3.2 Validating numerical results

It was shown in a previous study [28] that full-scale roll decay motion simulation strategy for the ship Bettica was reasonable and could be applied for other vessels. Although the DTC vessel represents a typical hull form for the container ship, it is not an operational container ship. As the full-scale ship is not built and there is no sea trial data of roll decay tests for DTC, the full-scale numerical results are not validated with sea trial data. This can result in unreasonable setting parameters of full-scale simulation and might be misunderstood as scale effects. Hence, to limit this risk, numerical parameters set for DTC at model-scale and full-scale are chosen as mentioned in section 2.2 so that the correspondence in the setting parameters between model-scale and full-scale simulation is ensured as recommended in previous study [28]. In this section, only the CFD result of model-scale is validated with the model test data (EFD result) to confirm the accuracy of numerical simulation. The experimental data of roll decay tests for DTC model can be found in the publication of Moctar et al. [13]. At different Froude numbers, roll decay tests of DTC model (hull with rudder and bilge keels) are simulated with defined time steps as mentioned in Table 2. Roll decay curves and extinction coefficients are used to compare with corresponding experimental data, in which EFD extinction coefficients are calculated from EFD roll decay curves. The error (E) can be defined as follows:

$$E = \frac{D - S}{S} 100\% \tag{10}$$

where D - numerical result and S - experimental result.

Figure 8 compares the numerical and experimental results of the roll decay motion of DTC model at different forward speeds. A comparison between CFD and EFD results of the extinction coefficient is given in Table 4, in which the extinction coefficients of three mesh solutions at zero Froude number are shown to justify the adequacy of mesh resolution. The results in Figure 8 show that there is a good agreement between numerical simulations and measurements. In Table 4, the errors E (%) of medium mesh cases are 6.023 %, 5.338 % and 4.788 % for F_r = 0, F_r = 0.105 and F_r = 0.192, respectively, which are acceptable in numerical simulation. The case of coarse mesh (F_r = 0) has the largest error of 19.164 %, which is not good to achieve the accurate result. The case of fine mesh (F_r = 0) has the lowest error of 3.746 %, however, it takes more time to calculate compared to the medium mesh case. As the number of cells of the fine mesh is twice that of the medium mesh, but the results are not much better, the medium mesh is utilized in subsequent study cases to optimize the computational time.

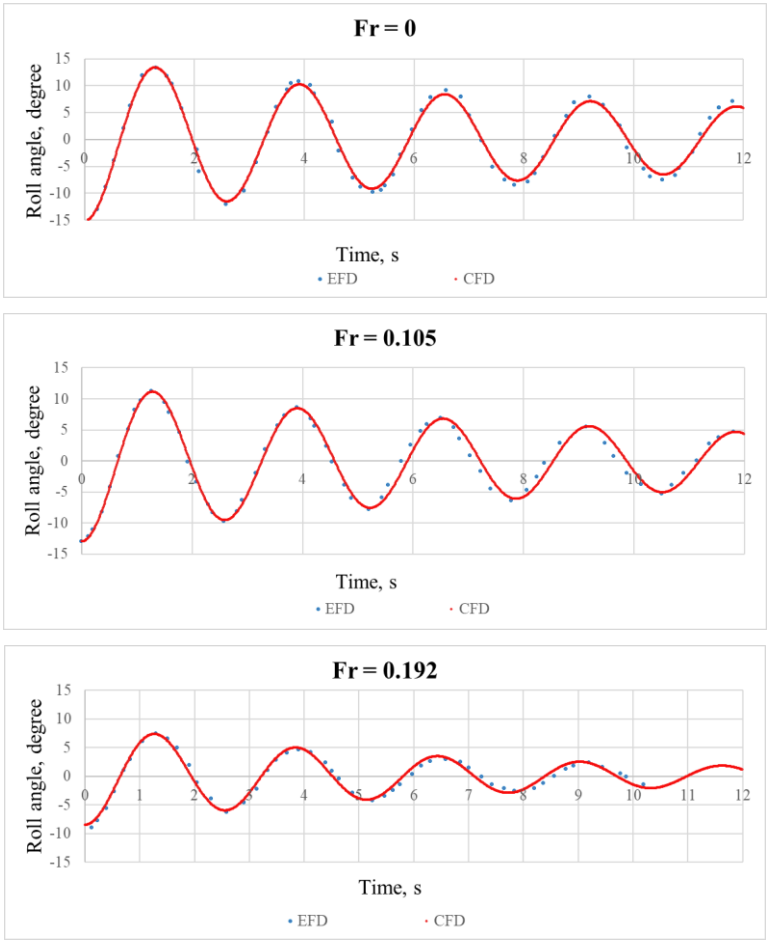

Fig. 8 The validation results of DTC model (medium mesh)

Table 4 Extinction coefficient and error E (%)

Froude number	Mesh type	CFD result	EFD result	*E* (%)
Fr = 0	Fine	0.0720	0.0694	3.746
Fr = 0	Medium	0.0736	0.0694	6.023
Fr = 0	Coarse	0.0827	0.0694	19.164
Fr = 0.105	Medium	0.0792	0.0752	5.338
Fr = 0.192	Medium	0.1291	0.1232	4.788

4. Results and discussions

4.1 Scale effects on roll motion through roll decay tests

This part presents the simulation of roll decay motion for the DTC vessel at model-scale and full-scale under various hull conditions (naked hull, hull with bilge keels (BK)) at various Froude numbers (*Fr* = 0; 0.06; 0.105; 0.192). Simulating conditions are applied the same for both the model and the ship to ensure the similarity between model-size and full-size simulations. As the roll amplitudes significantly depend on the setting parameters, the similarity between model-size and full-size in numerical simulation should be defined by the similarity of numerical setting parameters such as grid size, time step size, wall *y*+ and Courant number [28]. For the DTC vessel, the following parameters are set: medium mesh, time step with the Courant number smaller than 1.0, and wall *y*+ from 1 to 2.5 for model-scale and from 50 to 200 for full-scale. To compare model-scale to full-scale amplitudes, the time can be expressed in the same unit as t/T_r. Figure 9 shows the roll decay motions of the DTC vessel in comparison between model and ship. Here,

the words "model" and "ship" are used to indicate "model-scale" and "full-scale" in all graphs and subsequent descriptions, respectively. It is found that for both hull conditions, the roll amplitudes at both scales are different. The discrepancy in the roll amplitudes is observed more clearly in cases of F_r = 0 and low forward speed (F_r = 0.06), while it is not significant at higher speeds (F_r = 0.105 and F_r = 0.192).

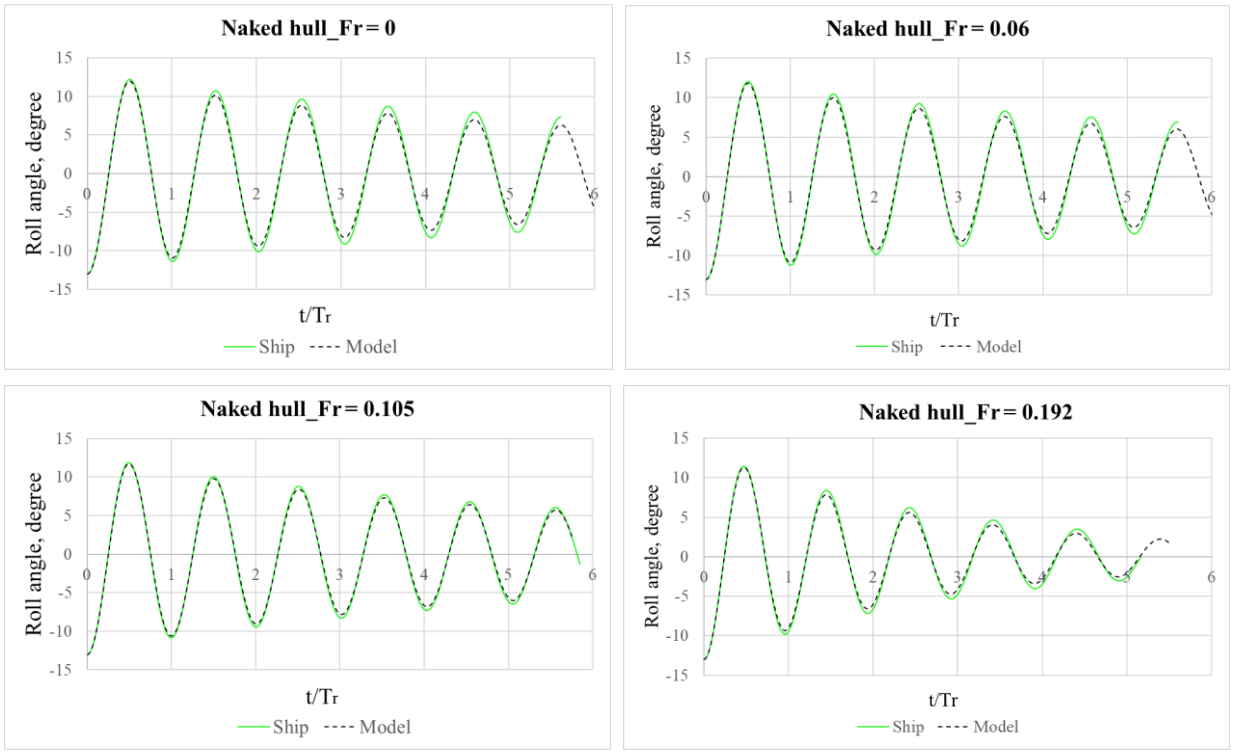

a) DTC naked hull

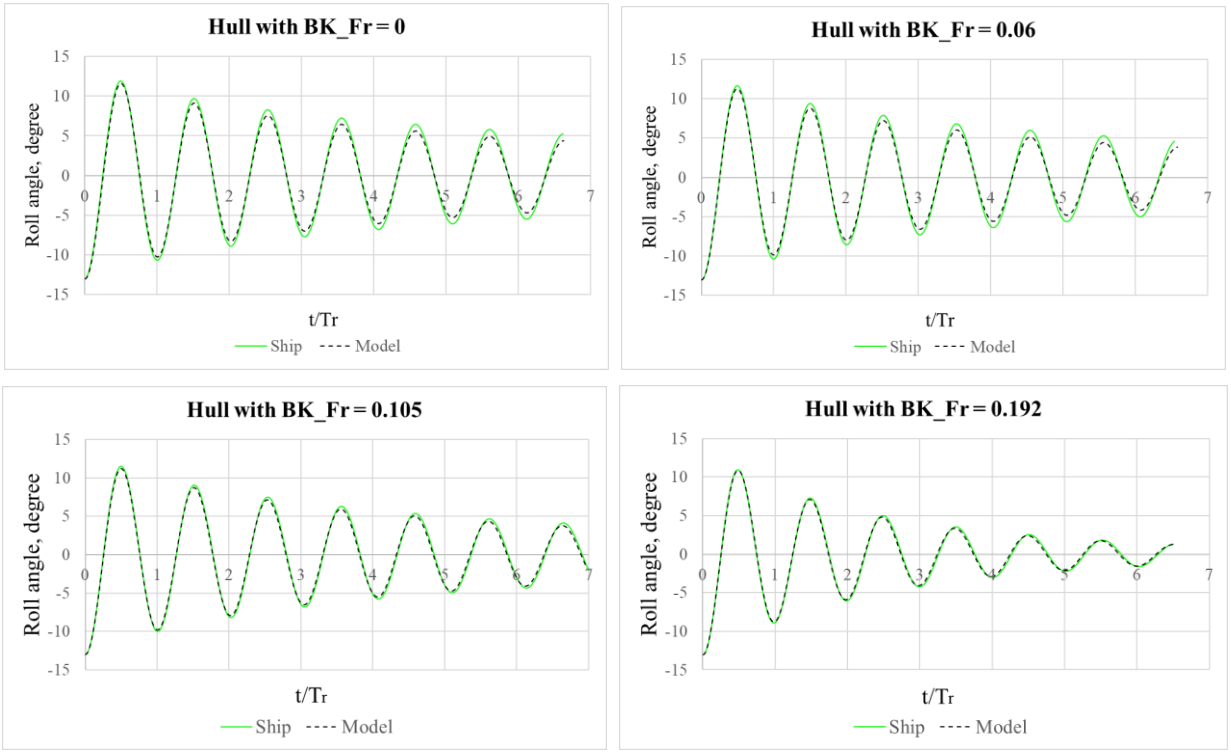

b) DTC hull with bilge keels

Fig. 9 Roll decay motions (compare between ship and model)

4.2 Clarification of scale effects on roll motion through forced roll tests

In previous a study on the Bettica ship [12], it was shown that besides the frictional damping component, the bilge keel damping component was affected by the scale effects when the height of bilge keel (h_{BK}) was too small. As the bilge keels installed on the DTC ship have a relatively short breadth compared to the ship's overall size, the bilge keel damping component might also be affected by the scale effects. Therefore, in this section, forced roll motions are simulated to clarify the impacts of vessel size on roll damping components of DTC vessel. Forced roll simulations of DTC ship (naked hull, hull with bilge keels) are performed at two forward speeds (Fr = 0.06 and Fr = 0.192) with the roll amplitude at 13 degrees. The numerical setting parameters are applied the same as in roll decay simulation, only the roll motion is set as forced roll motion.

From forced roll simulation results, the roll damping coefficient is calculated based on the method of B. Yildiz and T. Katayama [33]. In numerical simulation, the following harmonic oscillation is set for the overset region to model the forced roll motion:

$$\phi(t) = \phi_a \sin(\omega t) \tag{11}$$

where ϕ_a - roll amplitude, ω - roll angular frequency. Forced roll motion equation based on taking into consideration a function $f(t)$, which is used to prevent unstable transient flows at the initial calculation time steps, is defined as:

$$\phi(t) = f(t)\phi_0 sin(\omega t) \tag{12}$$

$$f(t) = \begin{cases} \frac{1}{2} sin\left(\frac{1}{4} \times \frac{\pi}{T} \times t - \frac{1}{2}\pi\right) + \frac{1}{2} (t < 4T) \\ 1 (t > 4T) \end{cases} \tag{13}$$

where T_r represents the natural roll period. Using Fourier series expansion, from the result of roll moments (M_E) recorded over time, the motion equation of roll moment is described as:

$$M_E(t) = M_0 sin(\omega t + \varepsilon) \tag{14}$$

where M_0 – amplitude of roll moment, ε – phase difference between the roll moment and amplitude. The forced roll motion function and the phase difference between roll moment and roll amplitude are described in Figure 10 and Figure 11.

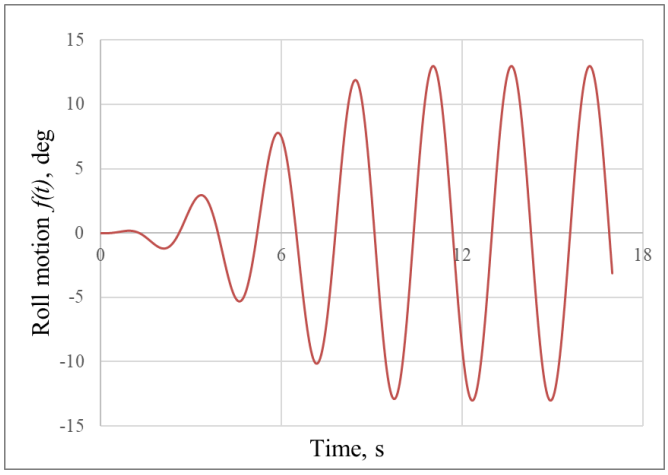

Fig. 10 Description of roll motion $f(t)$

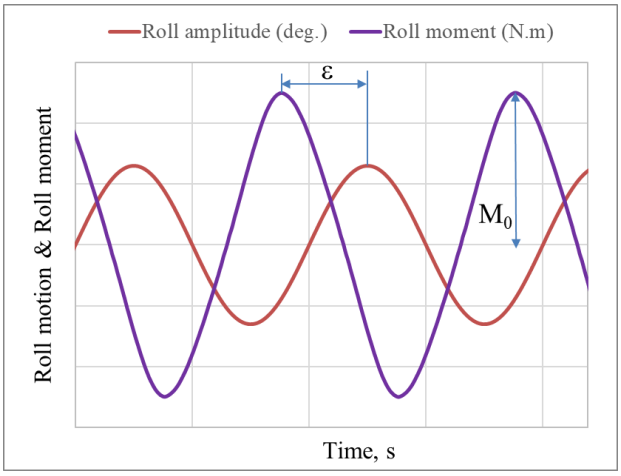

Fig. 11 Phase delay of roll moment to roll motion.

Then, total damping coefficient (b_{44}) and total damping coefficient in dimensionless form (B_{44}) are calculated as:

$$b_{44} = \frac{M_0 sin(\varepsilon)}{\phi_0 \omega}; \quad B_{44} = \frac{b_{44}}{\nabla \rho B^2} \sqrt{\frac{B}{2g}} \tag{15}$$

where ∇ - volume of displacement, g - gravity's acceleration, ρ - water density and B – moulded breadth of ship.

According to Ikeda's method [10], five components are assumed to create the roll damping: lift damping, frictional damping, eddy making, wave making, and bilge keel damping. As the amplitude of frictional moment (M_{0F}) and the phase angle between roll amplitude and frictional moment (ε_F) can be determined through simulation results, the frictional damping coefficient (B_{44F}) is calculated as:

$$B_{44F} = \frac{b_{44F}}{\nabla \rho B^2} \sqrt{\frac{B}{2g}}; \; b_{44F} = \frac{M_{0F} sin(\varepsilon_F)}{\phi_0 \omega} \tag{16}$$

For the ship with a round shape hull like DTC, the bilge keel damping coefficient (B_{44BK}) is defined as:

$$B_{44BK} = B_{44 \text{ with BK}} - B_{44 \text{ without BK}} \tag{17}$$

Other roll damping components such as lift damping (B_{44L}), wave making (B_{44W}) and eddy making (B_{44E}) are treated as a single coefficient and defined by:

$$B_{44W} + B_{44E} + B_{44L} = B_{44} - B_{44F} - B_{44BK} \tag{18}$$

The formulae of roll damping coefficients of different components are summarized in Table 5.

Table 5 Roll damping coefficient of difference damping components

Component	Dimensional	Non-dimensional
Friction damping coefficient	$b_{44F} = \frac{M_{0F} sin(\varepsilon_F)}{\phi_0 \omega}$	$B_{44F} = \frac{b_{44F}}{\nabla \rho B^2} \sqrt{\frac{B}{2g}}$
Bilge keel damping coefficient	$b_{44BK} = b_{44 \text{ with BK}} - b_{44 \text{ without BK}}$	$B_{44BK} = B_{44 \text{ with BK}} - B_{44 \text{ without BK}}$
Total of lift damping, wave making, eddy making coefficient	$b_{44W} + b_{44E} + b_{44L} = b_{44} - b_{44F} - b_{44BK}$	$B_{44W} + B_{44E} + B_{44L} = B_{44} - B_{44F} - B_{44BK}$
Total roll damping coefficient	$b_{44} = \frac{M_0 sin(\varepsilon)}{\phi_0 \omega}$	$B_{44} = \frac{b_{44}}{\nabla \rho B^2} \sqrt{\frac{B}{2g}}$

Figure 12 provides a comparison of roll damping coefficients of full-scale ship at zero forward speed between CFD and Ikeda's original method [34]. The roll damping coefficients and their contributions (%) at different Froude numbers and hull conditions are shown in Figure 13 and Figure 14. To get a more intuitive view of the difference of relative flow velocity for bilge keel height, the non-dimensional velocity fields in X direction (which is divided by the square root of the height of bilge keel) in the moment when the hull with rolling is upright are observed (see Figure 15). Figure 16 compares the non-dimensional turbulent kinetic energy (which is divided by the square of roll angular velocity) between model-scale and full-scale at different forward speeds in the upright position. Figure 17 shows the non-dimensional velocity vectors in YZ direction (which is divided by the roll angular velocity) compared model-scale to full-scale at different forward speeds in the upright position. Here, YZ is the direction that is perpendicular to the bilge keel surface. The position of the section, which is used to get the non-dimensional velocity magnitude and vector, is at 0.5 L_{pp}.

From Figure 12, it is seen that the roll damping coefficients of frictional and other components of full-scale ship calculated by both methods are similar, while the damping coefficients of the bilge keel

component obtained by CFD method have a disparity compared to Ikeda's method. The reason might be due to the effects of the shape of bilge keel related to its small breadth and thick thickness of its tip is not being considered in Ikeda's method. In addition, Ikeda's method also can not consider the effects of divided bilge keel, then it is assumed to be a plate. However, this result shows the similarity between two methods in naked hull condition, meaning that the numerical strategy used in this study is reasonable.

The results in Figure 13 and Figure 14 show that for both naked hull and hull with BK, B_{44F} of the model is larger than that of the ship. In addition, the proportion of the frictional component is larger at low Froude number. When the speed increases, the increase of lift damping makes the damping coefficient of other components (B_{44L} + B_{44E} + B_{44W}) increase. Therefore, although B_{44F} is larger than the case of low speed, its contribution drops to just 4-6 % in the model-scale and 1-3 % in the full-scale. In Figure 15, the full-scale and model-scale non-dimensional velocity fields at zero and low forward speeds appear distinctive. This explains why the frictional component experiences the larger scale effects at zero and low forward speeds. Comparing full-scale to model-scale, the ship generates a smaller total roll damping coefficient because the frictional damping coefficient is lower at higher Reynolds number for full turbulence flow.

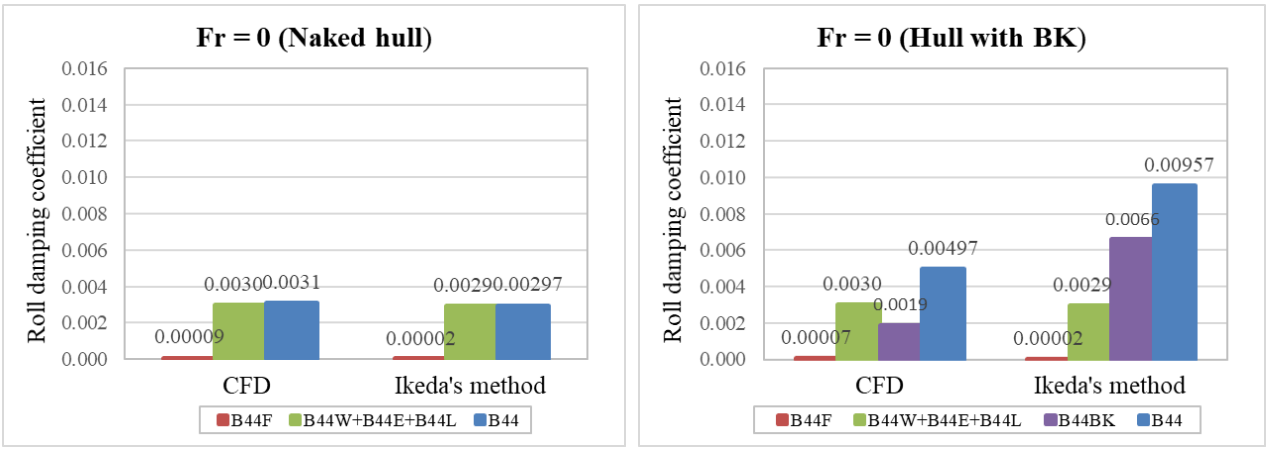

Fig. 12 Roll damping coefficients in dimensionless form of full-scale ship (compare CFD to Ikeda's original method)

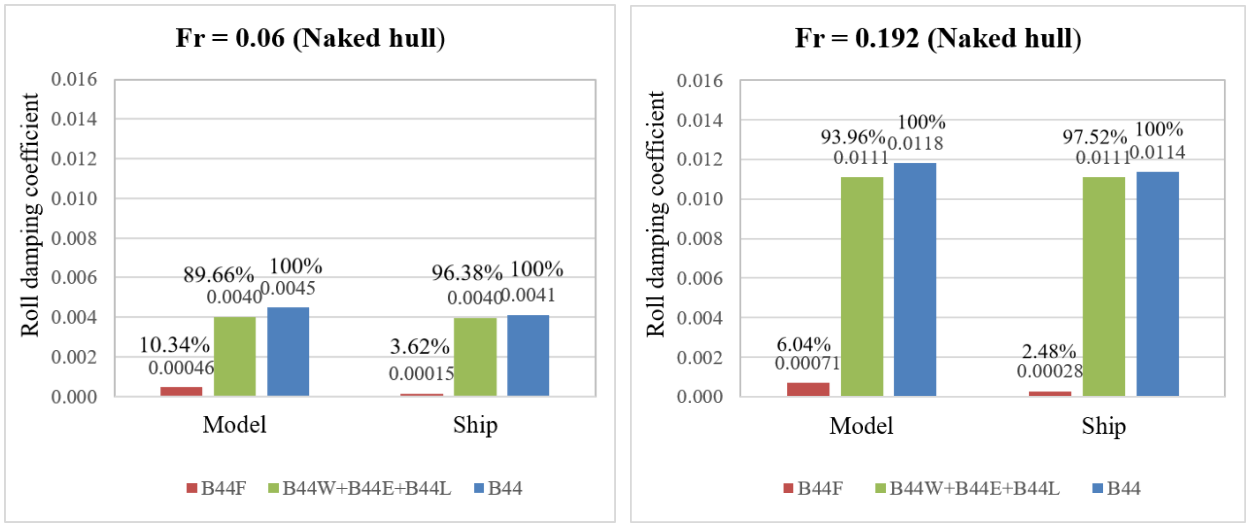

Fig. 13 Roll damping coefficients in dimensionless form and their contributions (Naked hull)

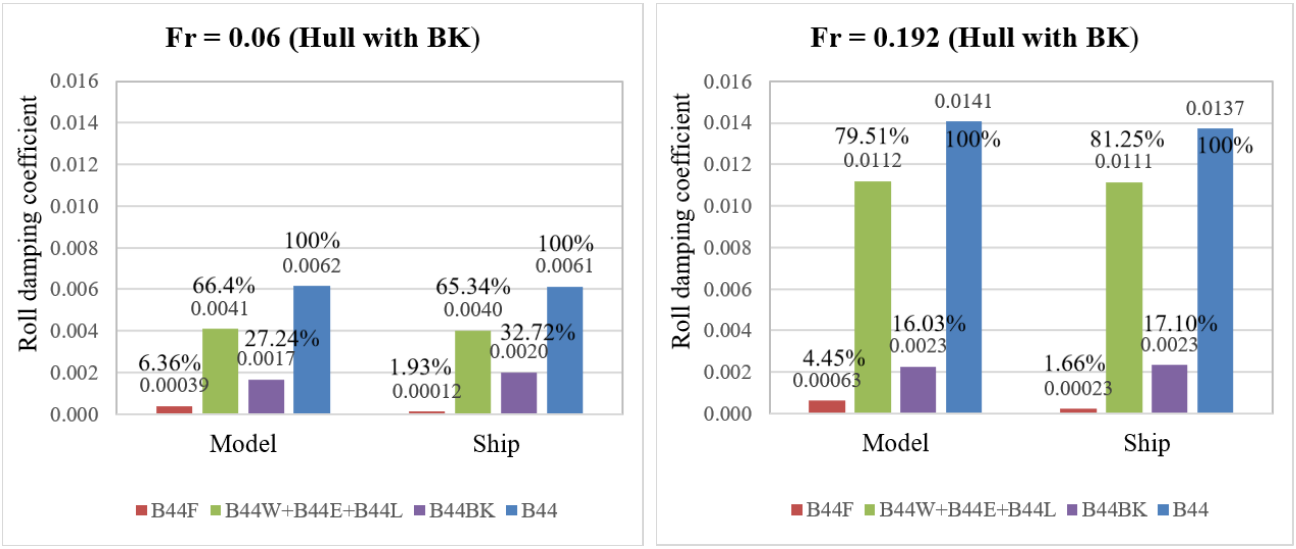

Fig. 14 Roll damping coefficients in dimensionless form and their contributions (Hull with BK)

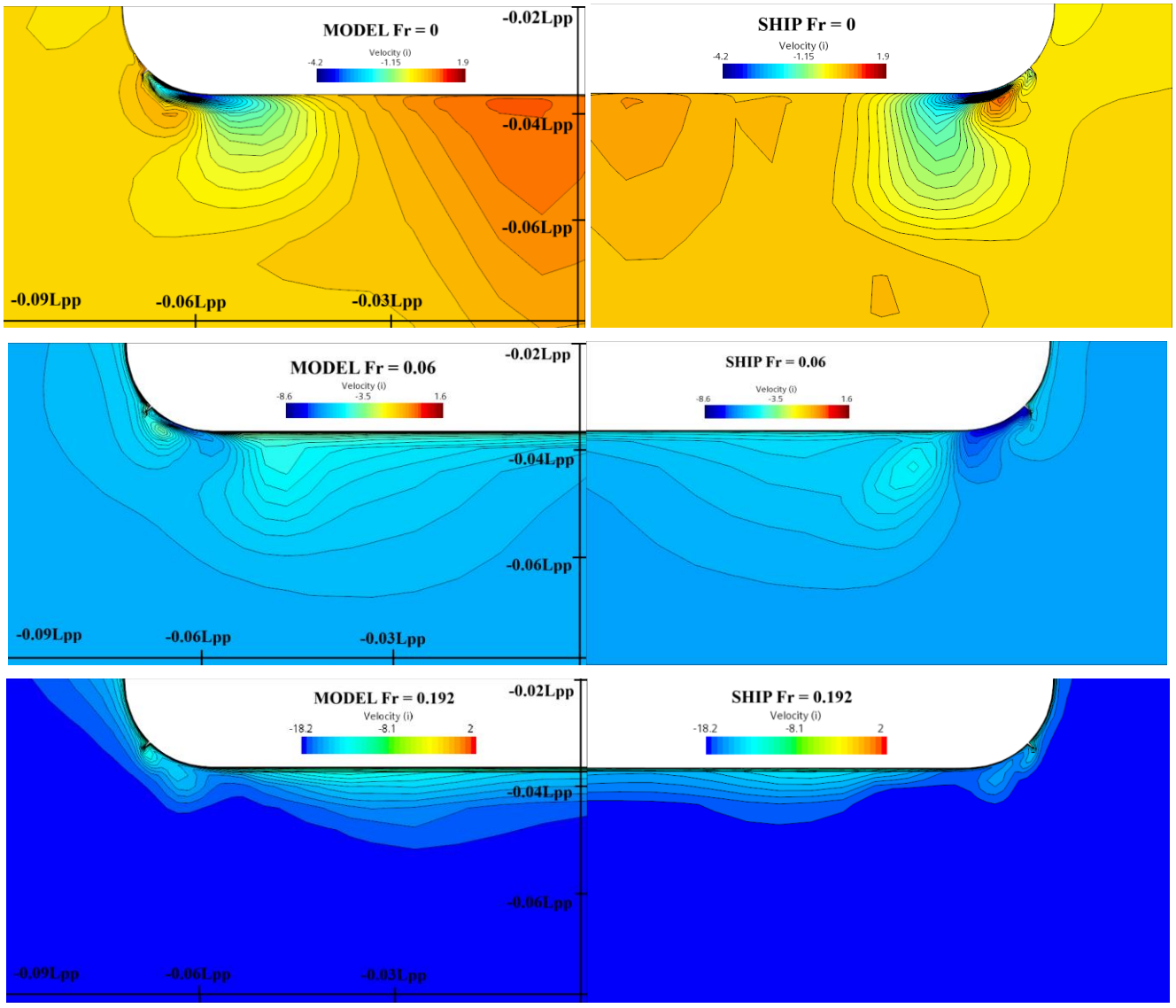

Fig. 15 Non-dimensional velocity field in *X* direction on earth fixed coordinate system of DTC ship and model (Hull with BK)

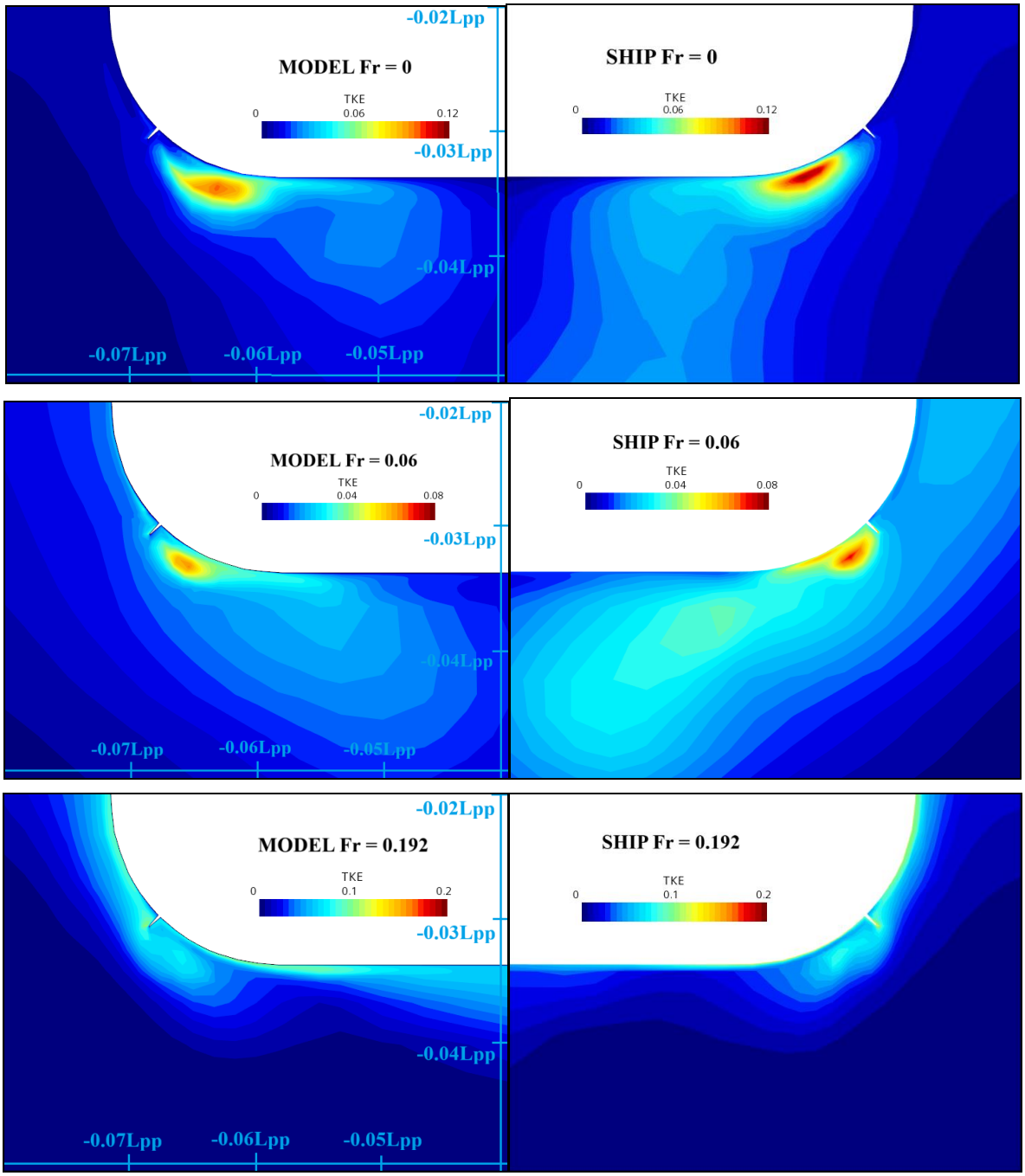

Fig. 16 Non-dimensional turbulent kinetic energy (on earth fixed coordinate system) of DTC ship and model (Hull with BK)

For hull with bilge keels, when forward speed is low, it is evident that scale effects have an impact on bilge keel damping. Specifically, full-scale B_{44BK} is larger than model-scale one, as shown in Figure 14. Figure 16 shows that the non-dimensional turbulent kinetic energy of full-scale is larger than that of model-scale at low Froude number, while it is similar at high Froude number. The increase in turbulent kinetic energy, which means the fluctuating velocity in turbulent flow is higher, leads to larger vortex sizes. This is because the energy cascade process in turbulence favours the growth and intensification of large-scale eddies. The evidence is in Figure 17, the size of vorticities created by the bilge keel of the ship is bigger than that of the model at low Froude number. In addition, the vorticity size at both scales at high Froude number is similar. This may prove that the non-dimensional relative velocity created by roll motion and forward speed affects the size of vorticities created by the bilge keel. In particular, the non-dimensional relative velocity of the model is lower than that of the ship, and the discrepancy between the relative velocities of both scales at low forward speed is also larger than that at high speed. This is believed to be the cause of the

impacts of vessel size on the bilge keel damping component. Therefore, detailed investigation of the flow field created by roll motion and forward speed is necessary.

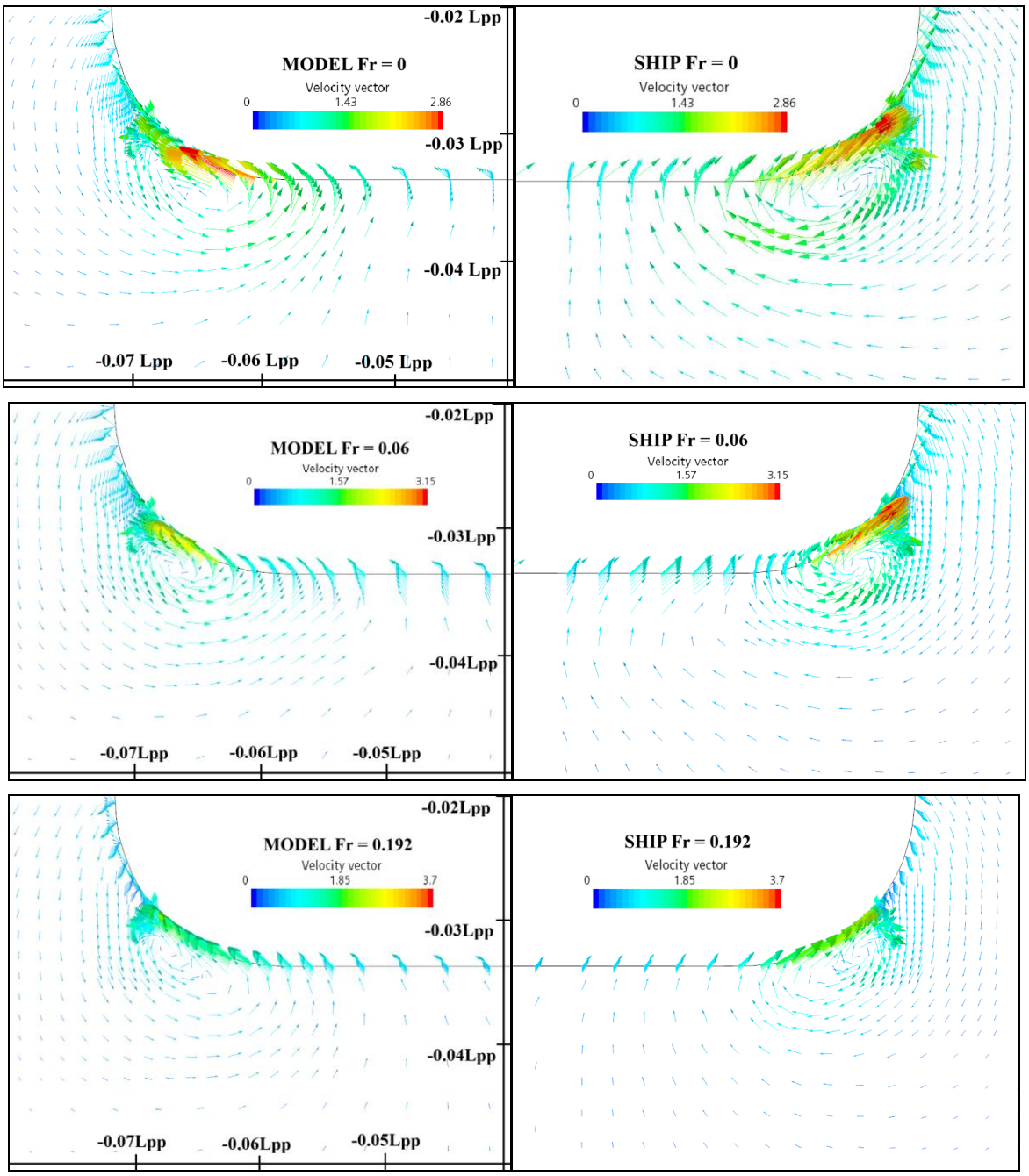

Fig. 17 Non-dimensional velocity vectors in *YZ* direction on earth fixed coordinate system of DTC ship and model (Hull with BK)

As the ship simultaneously experiences running and rolling, the boundary layer will be created by both roll motion and forward speed (FS). This differs from rolling with zero forward speed, which the velocity field and the boundary layer are only created by roll motion, as shown in the study of Y. Ikeda [35]. To investigate the flow field around naked hull created by roll motion and forward speed, the velocity distributions in different directions (*X* direction and *YZ* direction) at the position of the bilge keel (in the moment when ship with rolling is upright position) are exported and given in Figure 18 and Figure 19.

Figure 20 depicts the velocity distribution in *YZ* direction around naked hull created by only forward speed (without roll motion) and Figure 21 depicts the velocity distribution in *YZ* direction created by only roll motion (by subtracting the velocities in Figure 19 with ones in Figure 20). Here b/h_{BK}=1 in horizontal axis in Figure 18~21 represents the bilge keel tip, and the velocity distributions in these figures is of naked hull. Figure 22 shows the method to determine the velocity in *YZ* direction. To compare between ship and model, the velocity distribution is expressed as the non-dimensional value obtained by Equation 19:

$$\hat{V}_X = \frac{V_X}{V}; \hat{V}_{YZ} = \frac{V_{YZ}}{V_m} \tag{19}$$

where V – forward speed (m/s) and $V_m = r\omega\theta_0$ – roll angular velocity (m/s), b – distance from the observed point to the ship surface (m).

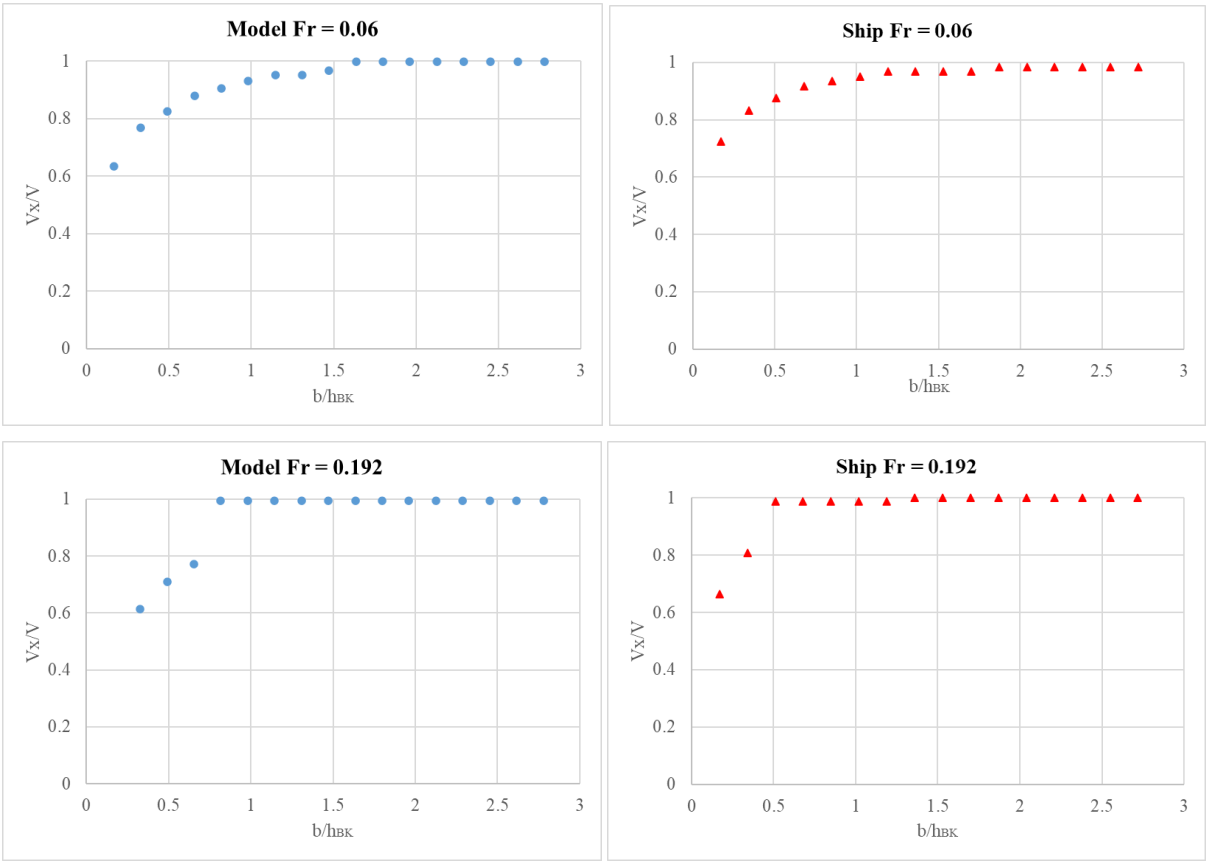

Fig. 18 Non-dimensional velocity distribution in *X* direction on earth fixed coordinate system caused by roll motion and different forward speeds (Naked hull)

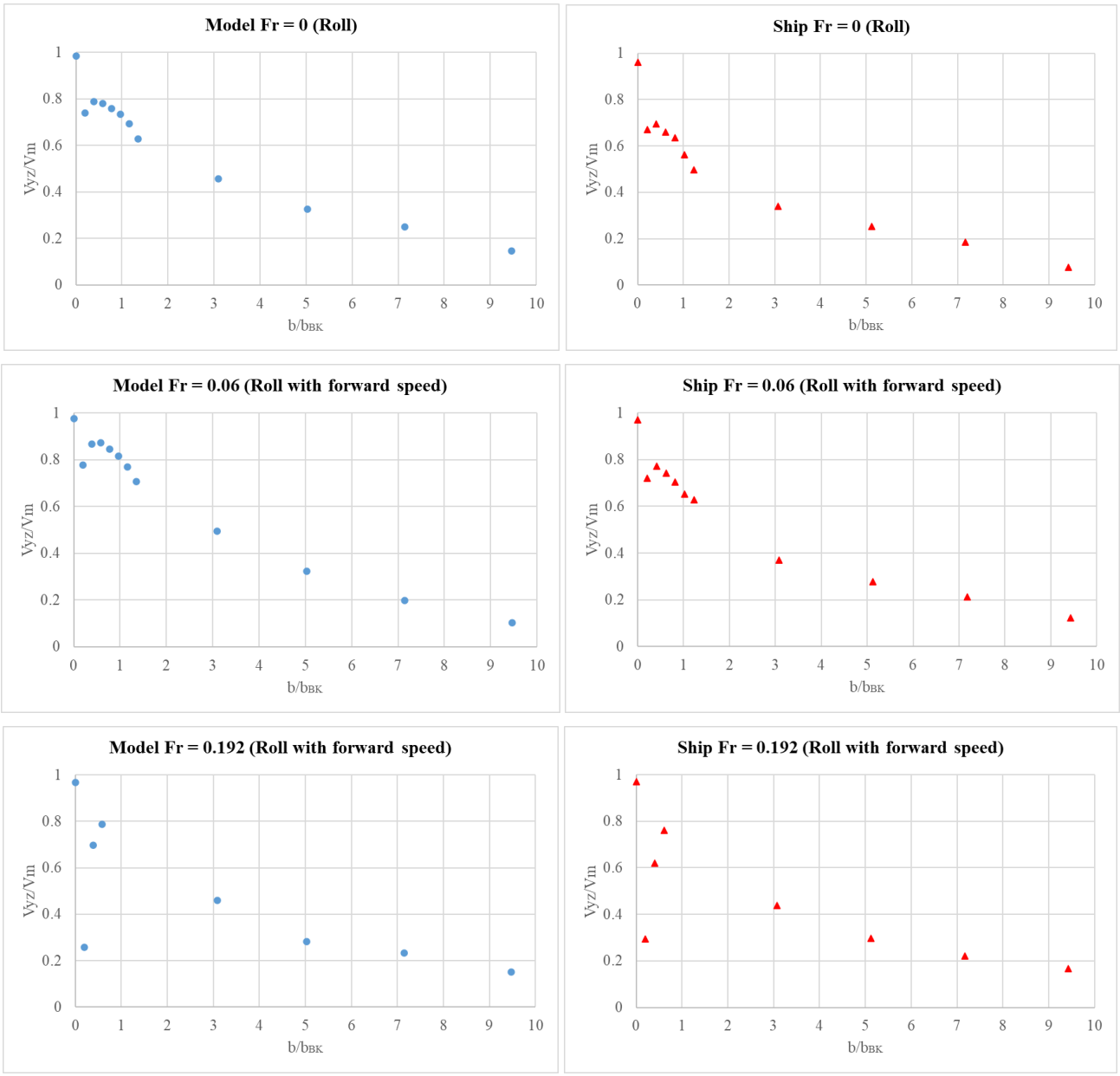

Fig. 19 Non-dimensional velocity distribution in *YZ* direction on earth fixed coordinate system at different forward speeds (roll with forward speed) (Naked hull)

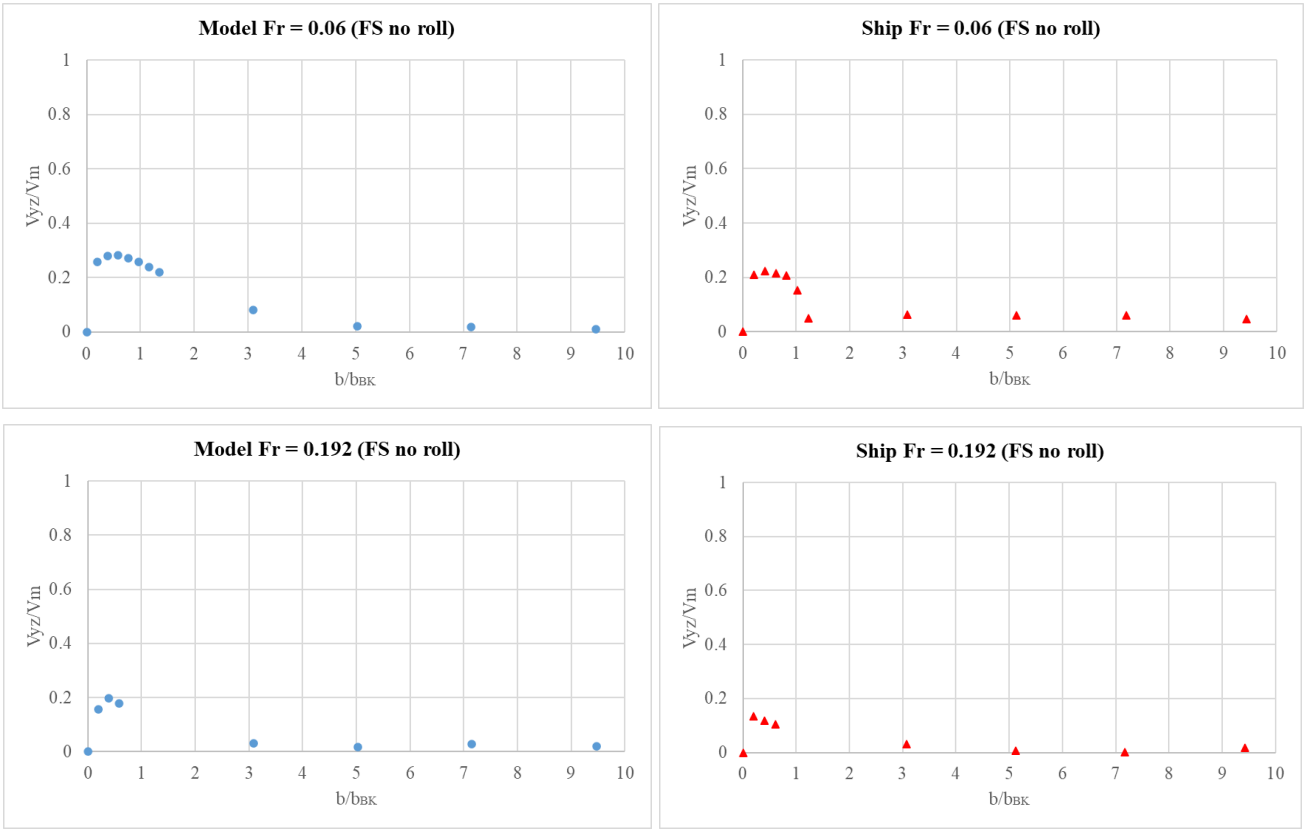

Fig. 20 Non-dimensional velocity distribution in *YZ* direction on earth fixed coordinate system around naked hull created by only forward speed without roll motion (Naked hull).

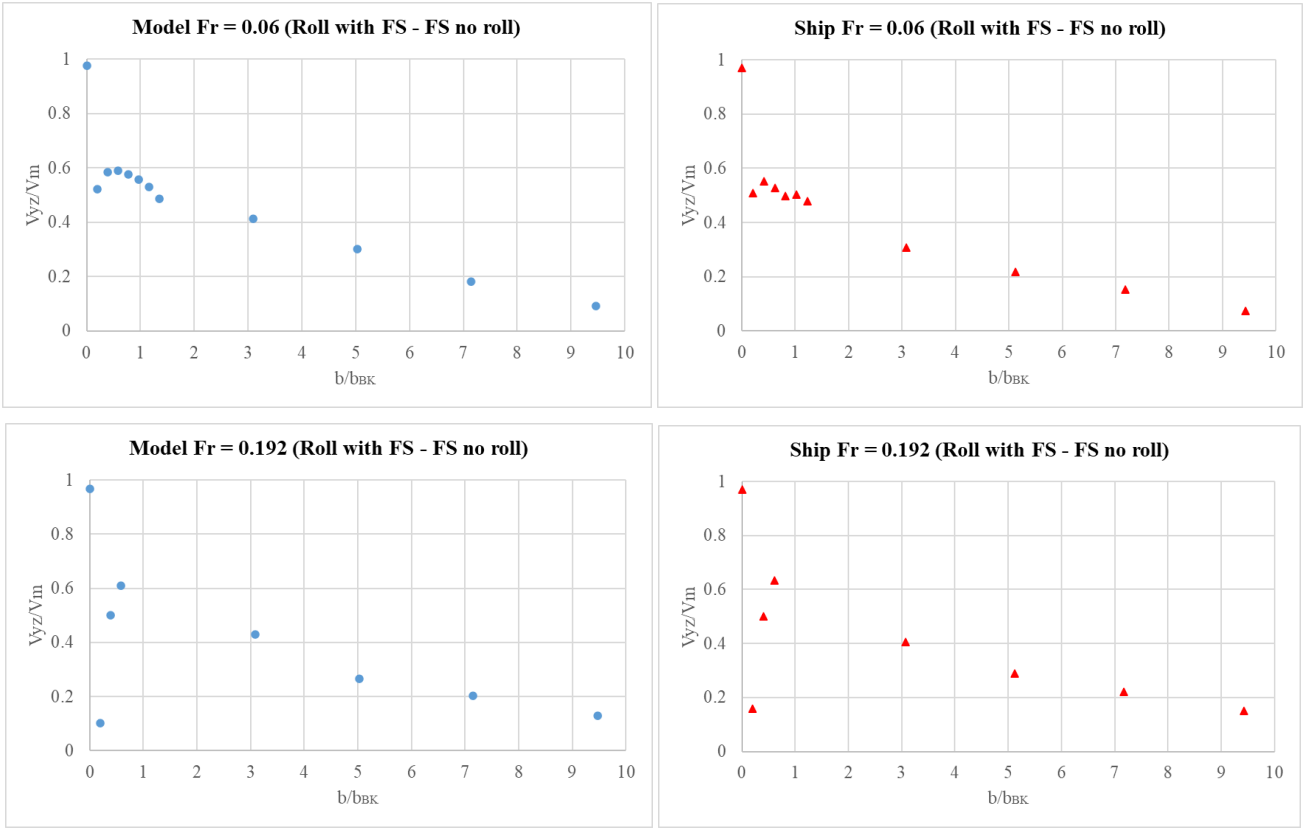

Fig. 21 Non-dimensional velocity distribution in *YZ* direction on earth fixed coordinate system created by roll motion which obtained by subtracting the velocities in Figure 19 with ones in Figure 20 (Naked hull).

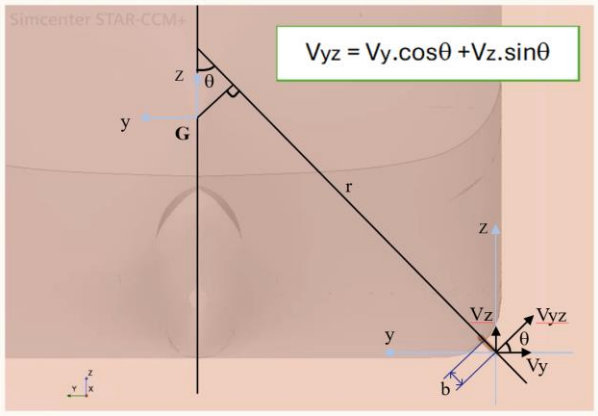

Fig. 22 Velocity in *YZ* direction

Observing the non-dimensional velocity distribution caused by only forward speed near the hull surface in Figure 18, it is noted that full-scale non-dimensional velocity magnitude by X direction is higher than model-scale one. In Figure 19, the non-dimensional velocity distribution in *YZ* direction caused by rolling and forward speed between the model and the ship is different at $Fr = 0$ and $Fr = 0.06$, while it is similar at $Fr = 0.192$. Figure 20 shows that when the ship runs without rolling, non-dimensional velocities in *YZ* direction become almost zero due to moving away from the hull. This indicates that non-dimensional velocities in *YZ* direction are affected by forward speed. Figure 21 shows the non-dimensional velocity distribution in *YZ* direction caused by only rolling at the condition ship with forward speed with rolling. The non-dimensional velocity distribution is obtained by subtracting the results shown in Figure19 from those in Figure 20. It is supposed that the non-dimensional velocity on the hull is 1.0 because of the non-slip condition and the velocity decreases according to the increase of distance from hull surface; however, the results are not necessarily consistent. Because there is the interaction of velocity extremely near the hull caused by forward speed and rolling, it is difficult to remove the interaction above-mentioned method, it is neglected in the following discussions.

From Figure 21, at low speed, the non-dimensional velocity at $b/h_{BK} = 1$ of the model is larger than that of the ship. Therefore, the non-dimensional relative velocity of fluid to the tip of the bilge keel of the model is smaller than that of the ship, leading to the smaller size of vorticity at model-scale. As a result, B_{44BK} of the model is also smaller. On the other hand, at high Froude number, the non-dimensional velocity at $b/h_{BK} = 1$ of the model is almost the same as that of the ship. Therefore, B_{44BK} of model-scale becomes the same as of full-scale. Hence, the appearance of forward speed is the reason for the increase in the non-dimensional velocities at the tip of the bilge keel of model-scale when the ship rolls with forward speed. In conclusion, the difference in the non-dimensional relative velocity distributions for the height (or breadth) of bilge keels between the model and ship can explain why bilge keel roll damping is influenced by the scale effects at low forward speed. On the other hand, it is believed that the difference in the boundary layer thickness between model and full-scale, as observed in Figure 15 might result in the smaller B_{44BK} of model-scale at low Froude number, as mentioned in previous studies [11], [12]. However, as determining the boundary layer thickness created by roll motion and forward speed remains an unsolved problem until the present, it should be studied more in the future.

5. Conclusions

This study investigates the effects of scale on rolling motion for a container vessel by simulating roll motions (roll decay and forced roll tests) at both full-scale and model-scale at varying forward speeds. Various components of damping coefficients are determined, and the flow field created by roll motion and forward speed surrounding bilge keels is analysed. Some important findings are derived as follows:

1. For roll decay motion, the scale effects (displayed in the disparity of roll amplitudes between model-scale and full-scale) tend to be slightly larger at zero and low forward speeds, but they are not substantial at higher speed.

2. Analysing various roll damping components through forced roll simulation, it is found that the frictional damping coefficient of the model is larger than that of the ship and the proportion of the frictional component is larger at low Froude number. In the case of low Froude number, scale effects have an impact on the bilge keel component, in which the full-scale B_{44BK} is slightly larger than the model-scale one.
3. Analysing the vorticity size and turbulent kinetic energy (Figure 16), it is found that the non-dimensional relative velocity created by roll motion and forward speed affects the size of vorticities created by the bilge keel. From the velocity profiles in different directions (Figure 18 to Figure 21), a discrepancy in the velocity distribution between two scales is observed when the ship rolls at low forward speed. The difference in the relative velocity distributions for the breadth of bilge keels between model-scale and full-scale explains why bilge keel roll damping is influenced by the scale effects at low forward speed.

In summary, the scale effects on roll motion are clarified and their causes are explained in detail in this paper. These findings can be used to improve the empirical or semi-empirical roll damping prediction method. However, the influence of the relationship between the bilge keel breadth and the boundary layer thickness created by roll motion and forward speed on the scale effects is still unclear. Therefore, a deeper insight into the boundary layer and clarification of the definition of the boundary layer are necessary in future studies.

ACKNOWLEDGEMENT

This work was financially supported by JST SPRING, Grant Number JPMJSP2139.

REFERENCES

[1] Zhang, H., Chen, X., Liu, H., Wang, X., 2018. Scale Effect Studies on Hydrodynamic Performance for DTMB 5415 Using CFD. *International Conference on Offshore Mechanics and Arctic Engineering*, American Society of Mechanical Engineers, https://doi.org/10.1115/OMAE2018-77331

[2] Song, K., Guo, C., Wang, C., Sun, C., Li, P., Zhong, R., 2020. Experimental and numerical study on the scale effect of stern flap on ship resistance and flow field. *Ships and Offshore Structures*, 15(9), 981-997. https://doi.org/10.1080/17445302.2019.1697091

[3] Dogrul, A., Song, S., Demirel, Y.K., 2020. Scale effect on ship resistance components and form factor. *Ocean Engineering*, 209, 107428. https://doi.org/10.1016/j.oceaneng.2020.107428

[4] Dogrul, A., 2022. Numerical Prediction of Scale Effects on the Propulsion Performance of Joubert BB2 Submarine. *Brodogradnja*, 73(2), 17-42. https://doi.org/10.21278/brod73202

[5] Ma, Z., Ji, N., Deng, X., Shi, C., 2024. Influence of scale effect on flow field offset for ships in confined waters. *Brodogradnja*, 75(1), 1-22. https://doi.org/10.21278/brod75106

[6] Grant, D. J., 2008. Full Scale Investigation of Bilge Keel Effectiveness at Forward Speed. *M.Sc. Thesis*. Faculty of Virginia Polytechnic Institute and State University, Blacksburg, Virginia.

[7] Broglia, R., Bouscasse, B., Di Mascio, A., Lugni, C., Atsavapranee, P., 2009. Experimental and numerical analysis of the roll decay motion for a patrol boat. *Nineteenth International Offshore and Polar Engineering Conference*, *ISOPE*, June 21-26, Osaka, Japan.

[8] Söder, C. J, Rosén, A., Werner, S., Huss, M., Kuttenkeuler, J., 2019. Assessment of ship roll damping through full-scale and model-scale experiments and semi-empirical methods. *Fluid Mechanics and Its Applications*, vol 119, Springer, Cham. https://doi.org/10.1007/978-3-030-00516-0_10

[9] Kianejad, S., Enshaei, H., Duffy, J., Ansarifard, N., Ranmuthugala, D., 2018. Investigation of scale effects on roll damping through numerical simulations. *Proceedings of the 32nd symposium on naval hydrodynamics*, 5-10 August, Hamburg, Germany.

[10] Ikeda, Y., Himeno, Y., Tanaka, N., 1978. Components of roll damping of ship at forward speed. *Journal of the society of Naval Architects of Japan*, 143, 113-125. https://doi.org/10.2534/jjasnaoe1968.1978.113

[11] Katayama, T., Kankaku, M., Yildiz, B., Sugimoto, K., Fukumoto, Y., 2021. Characteristics of Roll Damping of Pure Car Carrier and Liquefied Natural Gas Carrier and Applicability of Ikeda's Method with some Modifications. *Proceedings of the 1st International Conference on the Stability and Safety of Ships and Ocean Vehicles*, 7-11 June, Glasgow, Scotland, UK.

[12] Phuong, N.T.H., Yoshida, N., Taniguchi, T., Katayama, T., 2024. Investigation of the Scale Effects on Roll Motion for The Ship Bettica Using Numerical Simulation. *Polish Maritime Research*, 31(2), 4-12. https://doi.org/10.2478/pomr-2024-0016

[13] Moctar, O., Shigunov, V., Zorn, T., 2012. Duisburg Test Case: Post-Panamax Container Ship for Benchmarking. *Ship Technology Research*, 59(3), 50-64. https://doi.org/10.1179/str.2012.59.3.004

[14] Yong, Z., Zhi, Z., Li, Z., Tianlin, W., 2015. Turbulence model investigations on the boundary layer flow with adverse pressure gradients. *Journal of Marine Science and Application*, 14(2), 170–174. https://doi.org/10.1007/s11804-015-1303-0

[15] Guilmineau, E., Deng, G., Leroyer, A., Queutey, P., Visonneau, M., Wackers, J., 2015. Influence of the turbulence closures for the wake prediction of a marine propeller. *Fourth International Symposium on Marine Propulsors, SMP'15*, 30 May, Austin, United States.

[16] Jaouen, F., Koop, A.H., Vaz, G., Crepier, P., 2011. RANS predictions of roll viscous damping of ship hull sections. *IV International Conference on Computational Methods in Marine Engineering (MARINE)*, 28-30 September, Lisbon, Portugal, 76-93.

[17] Liang, L., Baoji, Z., Hao, Z., Jiaye, G., Zheng, T., Shuhui, G., Yuanbiao, B., Xu, Z., 2024. Study on numerical simulation and mitigation of parametric rolling in a container ship under head waves. *Brodogradnja*, 75(3), 1-19. https://doi.org/10.21278/brod75305

[18] Sadeghi, M.S., Hajivand, A., 2020. Investigation the effect of canted rudder on the roll damping of a twin-rudder ship. *Applied Ocean Research*, 103, 102-324. https://doi.org/10.1016/j.apor.2020.102324

[19] Menter, F., Ferreira, J.C., Esch, T., Konno, B., 2003. The SST turbulence model with improved wall treatment for heat transfer predictions in gas turbines. *Gas Turbine Congress (International) Proceedings*, 2-7 November, Tokyo, Japan. IGTC2003):059.

[20] Karim, M.M., Rahman, M.M., Alim, M.A., 2011. Performance of SST k-ω turbulence model for computation of viscous drag of axisymmetric underwater bodies. *International Journal of Engineering Transactions B: Applications*, 24(2), 139–146.

[21] Irkal, M. A. R., Nallayarasu, S., Bhattacharyya, S.K., 2019. Numerical prediction of roll damping of ships with and without bilge keel. *Ocean Engineering*, 179, 226–245. https://doi.org/10.1016/j.oceaneng.2019.03.027

[22] Ghamari, I., Mahmoudi, H.R., Hajivand, A., Seif, M.S., 2022. Ship Roll Analysis Using CFD-Derived Roll Damping: Numerical and Experimental Study. *Journal of Marine Science and Application*, 21, 67-79. https://doi.org/10.1007/s11804-022-00254-1

[23] Mancini, S., Begović, E., Day, A.H., Incecik, A., 2018. Verification and validation of numerical modelling of DTMB 5415 roll decay. *Ocean Engineering*, 162, 209-223. https://doi.org/10.1016/j.oceaneng.2018.05.031

[24] ITTC, 2014. Practical Guidelines for Ship CFD Applications. *Recommended Procedures and Guidelines*, No. 7.5-03-02-03. https://ittc.info/media/4196/75-03-02-03.pdf (accessed on 20th September 2024)

[25] Song, S., Demirel, Y. K., Atlar, M., 2019. An investigation into the effect of biofouling on the ship hydrodynamic characteristics using CFD. *Ocean Engineering*, 175, 122–137. https://doi.org/10.1016/j.oceaneng.2019.01.056

[26] Song, K., Guo, C., Sun, C., Wang, C., Gong, J., Li, P., Wang, L., 2021. Simulation strategy of the full-scale ship resistance and propulsion performance. *Engineering Applications of Computational Fluid Mechanics*, 15(1), 1321–1342. https://doi.org/10.1080/19942060.2021.1974091

[27] Terziev, M., Tezdogan, T., Incecik, A., 2022. Scale effects and full-scale ship hydrodynamics: A review. *Ocean Engineering*, 245. https://doi.org/10.1016/j.oceaneng.2021.110496

[28] Phuong, N.T.H., Taniguchi, T., Katayama, T., 2023. Numerical simulation strategy of full-scale ship roll decay motion. *JASNAOE conference proceedings, The Japan Society of Naval Architects and Ocean Engineers*, 27-28 November, Nagasaki, Japan. https://doi.org/10.14856/conf.37.0_365

[29] Mikulec, M., Piehl, H., 2023. Verification and validation of CFD simulations with full-scale ship speed/power trial data. *Brodogradnja*, 74 (1), 41-62. https://doi.org/10.21278/brod74103

[30] Roache, P. J., 2002. Code verification by the method of manufactured solutions. *The Journal of Fluids Engineering*, 124(1), 4–10. https://doi.org/10.1115/1.1436090

[31] ITTC, 2021. Uncertainty Analysis in CFD Verification and Validation Methodology and Procedures. *Recommended Procedures and Guidelines*, No. 7.5-03-01-01. https://www.ittc.info/media/9765/75-03-01-01.pdf (accessed on 20th September 2024)

[32] Yang, B., Wang, Z., Wu, M., 2012. Numerical simulation of Naval ship's roll damping based on CFD. *Procedia Engineering*, 37, 14-18. https://doi.org/10.1016/j.proeng.2012.04.241

[33] Yildiz, B., Katayama, T., 2017. Bilge keel–free surface interaction and vortex shedding effect on roll damping. *Journal of Marine Science and Technology*, 22, 432-446. https://doi.org/10.1007/s00773-016-0423-9

[34] Ikeda, Y., Himeno, Y., Tanaka, N., 1982. Prediction method of roll damping. Report of Department of Naval Architecture, Osaka Prefecture University.

[35] Ikeda, Y., Fujiwara, T., Himeno, Y., Tanaka, N., 1979. Velocity Field around Ship Hull in Roll Motion. *Journal of the Kansai Society of Naval Architects*, 171, 33-45. https://doi.org/10.14856/kansaiks.171.0_33